

Wave propagation in a nonlocal prestressed piezoelectric polygonal plate with non-homogeneity and hygroscopic effect

Rajendran Selvamani^{*1}, Hepzibah Christinal¹ and Farzad Ebrahimi²

¹Department of Mathematics, Karunya Institute of Technology and Sciences,
Coimbatore-641114, Tamilnadu, India

²Department of Mechanical Engineering, Imam Khomieni International University,
Qazvin 34148-96818, Iran

(Received April 13, 2022, Revised May 18, 2023, Accepted May 19, 2023)

Abstract. The humid thermal vibration characteristics of a nonhomogeneous thermopiezoelectric nonlocal plate of polygonal shape are addressed in the purview of generalized nonlocal thermoelasticity. The plate is initially stressed, and the three-dimensional linear elasticity equations are taken to form motion equations. The problem is solved using the Fourier expansion collocation method along the irregular boundary conditions. The numerical results of physical variables have been discussed for the triangle, square, pentagon, and hexagon shapes of the plates and are given as dispersion curves. The amplitude of non-dimensional frequencies is tabulated for the longitudinal and flexural symmetric modes of the thermopiezoelectric plate via moisture and thermal constants. Also, a comparison of numerical results is made with existing literature, and good agreement is reached.

Keywords: humidity; nonlocal stress-strain relation; piezoelectric resonator plate; polygonal shape

1. Introduction

The effects of humidity can be reduced by controlling the source of moisture, ventilation, and also by increasing the temperature. The physical properties of a material like stress and strain, displacement, thermal conduction, and electric conduction will vary when they are either in the presence or absence of water. Also, the dimensions and weight of the material will play a vital role during the construction. The piezoelectric materials will produce electricity when they are stressed and strained, and they will also undergo some other mechanical properties. Also, the plates will vibrate at a high frequency. Hence, humidity can have an enormous effect when it is on the piezoelectric plate, which leads to the construction of composite materials. These types of composite materials are used in the construction of actuators, sensors in marine engineering, and aerospace.

Adams and Keith Miller (1977) considered the elastic and transversely isotropic fiber and presented the influence of the thermal effect and moisture absorption on the fiber using the finite

*Corresponding author, Professor, E-mail: selvam1729@gmail.com

element numerical analysis. Hou fu *et al.* (2008) constructed the compact general solution of five mono harmonic functions and constructed the field for the point source heat for the semi-infinite transversely isotropic electro magneto thermo elastic material. Selvamani and Ponnusamy (2013a, 2013b) computed the frequencies, elastic variables and phase velocity for PZT-4 material and gave the plots for dispersion curves for the various ratio of the fluid wherein the piezoelectric plate is immersed. Also they analysed the generalized thermo elastic waves in a rotating ring shaped circular plate which is immersed in an in viscid fluid and introduced the two displacement potential functions to uncouple the equations of motion. They discussed the numerical results for the Zinc material and concluded that the waves were more dispersive and realistic when the thermal relaxation time, fluid and rotation parameter were present. Hutchinson (1979) found the approximate solution for the thick circular plates including shear and rotating effects and compared with the accurate series solution using three dimensional equations of linear elasticity theory. Chakraverty *et al.* (2005) used Rayley Ritz method to find the effect of non-homogeneity on elliptic plates and presented the numerical results using convergence test and validated with the available results. Shear deformation theories are tested for the static and free vibration analysis of new type of sandwich structures (Hanifi Hachemi Amar *et al.* 2023, Djilali *et al.* 2022, Kouider *et al.* 2021).

Bin *et al.* (2008) illustrated the influence of electric and magnetic effect on the non-homogeneous magneto-electro-elastic plates using the Legendre orthogonal polynomial series expansion. Selvamani and Infant Sujitha (2018a) analysed and presented the effect of thermo electromagnetic of nonhomogeneous poly plate numerically and graphically using linear elasticity theory. Also they (2018b) exhibited the numerical and graphical results for the wave propagation in a magneto thermo electroelastic disc of various shapes which was submerged in water. Chen *et al.* (2005) found the two types of vibrations such as elastic property and coupling effects on the non-homogeneous plate and also derived the numerical results. Jiyangi *et al.* (2006) discussed the influence of functionally graded factor on the multi-layered plates using state-space method with different stacking sequence. Pan (2001) considered the multilayered plates which are simply supported and exhibited the numerical examples for the effect of piezoelectric and piezomagnetic under the surface and internal loads. Selvamani (2015) considered the rotating polygonal cross sectional disc and derived the frequency equations for two particular cases (i) with fluid and without rotation (ii) without fluid and rotation. Also he (2017) presented the stress wave propagation in a thermo elastic plate with different shapes of inner and outer cross sections. Kakar (2013) found the great effects of the reinforcement gravity and magnetic field of the wave propagation on the prestressed half space using Whittaker foundation. Zhang and Yu (2013) studied the effects of initial stress on the guided wave propagation using Legendre orthogonal polynomial series expansion method. He also discussed the displacement and stress distribution on the plate. Selvamani and Ponnusamy (2015) discussed the free wave propagation in a piezothermo elastic rotating bar and the longitudinal and flexural equations for the PZT-5A material were studied analytically. Gawin *et al.* (199) exposed the computational analysis on the performance of hygro thermal and mechanical properties of concrete structures which were at high temperature using finite element and finite difference methods.

Vinyas and Kattimani (2017, 2018) used FEM to study the electromagnetic static and coupling result of a hygroscopic plate. Loghman *et al.* (2017) analysed the various effects of the material properties through power law moduli in radial mode of the functionally graded cylinder and he found that the radial displacement and the circumferential displacement were reacting inversely each other when the power index of the materials were increased. Zenkour (2012) developed the

analytical solution to the inhomogeneous hollow cylinder with the temperature gradient and represented the nonhomogeneity inclusion on the numerical results graphically. Vinyas *et al.* (2018) studied the effect of hygrothermal surrounding on the free vibration of magneto electro elastic plates and revealed the result that the temperature and the moisture affected the stiffness of the plate and showed that the free vibration has been affected extremely. Wang *et al.* (2004) carried out the deep study on the responses of histories and distribution of inter laminar stresses in the rectangular laminated plates with piezoelectric component layers in hygro thermal environment. Reddy and Chin (2007) used the power law distribution and first order shear deformation theory to study the thermo mechanical responses of functionally graded and cylinders.

Mehditabar *et al.* (2017) applied two kinds of numerical methods to solve the thermo elastic problem of functionally graded piezoelectric rotating hollow cylinder and plotted the stress values in mechanical structures. Selvamani (2016) considered the circular bar loaded with the thermal potential and compared the temperature distribution of longitudinal and flexural waves through the dispersion curve for symmetric and anti-symmetric mode. Jafari *et al.* (2012) analyzed the electro mechanical behavior of functionally graded piezoelectric hollow cylinder theoretically using the separation of variables and complex Fourier series. Ramu *et al.* (2018) investigated the numerical results of free vibration of the FGM plate in the hygrothermal environment. They formed the FGM plate based on the third order shear deformation theory and investigated the performance of natural frequencies of the FGM plates under the moisture and temperature conditions. Recently Janson *et al.* (2020) considered the EMC material and discussed the effect of temperature and humidity on the diffusivity of moisture constant. They have concluded that the moisture concentration is providing the nonlinear variation slightly when the humidity level is increasing at various points of moisture concentration. Contribution of dynamics of hygro thermo mechanical fields is notable in structural responses (Zaitoun *et al.* 2022, Mudhaffar *et al.* 2021, Al-Osta *et al.* 2021). Also Vinayak *et al.* (2021) investigated the vibration characteristics of LCS sandwich plates due to temperature and moisture using artificial neural network technique. They have presented the several numerical results conferred to figure out the influence of temperature and moisture on the LCS plates. The influence of surrounded foundation effects on the materials are exposed very well by several researchers (Bounouara *et al.* 2023, Mudhaffar *et al.* 2023, Tounsi *et al.* 2023, Belbachir *et al.* 2023, Bennedjadi *et al.* 2023, Hadji *et al.* 2023, Bot *et al.* 2022, Hebali *et al.* 2022, Bouafia *et al.* 2021).

Idea of size dependent effect (nonlocal) which motivates the mechanical and thermal character of materials is utilized by variety of researchers and scientists. To show case this, classical and non-classical vibration problems are added with nonlocal theory of elasticity. Adding non local parameter in motion equations amplify the micro level impact of materials. In local theory of elasticity the stress is confined to a single point of system whereas in non-local elasticity theory the elasticity is global and independent of single point theory. In this regard, Sing and Parveen (2020) investigated the effect of nonlocal parameter in an isotropic thermo elastic solid with two temperature. They used the Fourier and Laplace Transforms to solve the governing equations. Dastjerdi *et al.* (2021) analyzed the nonlocal effect on the thick porous functionally graded plates in the thermal and humidity environment. The semi analytical polynomial method has been used to solve the stress and strain equations and the numerical results have been validated with the available results. The plane wave solutions of the P, thermal and SV waves with distinct speeds have been derived using Lord Shulman theory in the insulated or isothermal boundary of a thermo elastic solid half space by Baljeet Singh and Rupender (2020). The graphical representation of the effect of nonlocal parameter on the speeds and energy ratios of reflected waves also have been

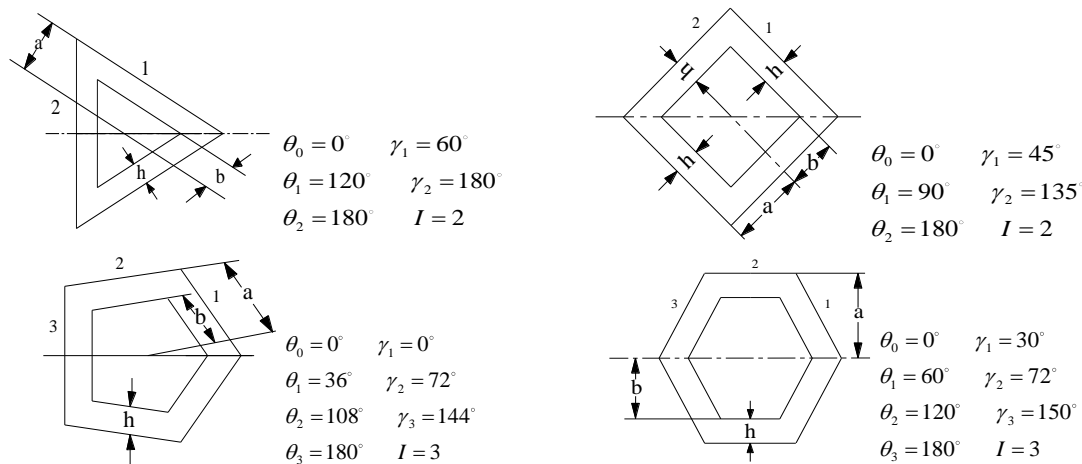


Fig. 1 Construction of poly plates

presented by them. Parveen Lata and Sukhveer Singh (2022) discussed the effect of rotation and inclined load in a nonlocal magnetothermoelastic solid with two temperature. Ibrahim *et al.* (2022) introduced nonlocal heat conduction approach in biological tissue generated by laser irradiation.

The effect of humidity and the nonlocal elasticity on the piezoelectric nonhomogeneous plate of polygonal cross sections are analyzed in this paper. The plate is under hydrostatical stress. The solution of this problem is found by the two kinds Bessel function. The boundary conditions and frequency equations are evaluated using the FECM. The numerical results of humidity on the considered plate is derived and plotted for the various cross sections of the plate such as Triangle, Square, Hexagon and Pentagon.

2. Fundamental equations and formulation of the model.

The hydrostatical thermo piezoelectric nonhomogeneous poly plate is depicted in Fig. 1. According to Eringen (1981) nonlocal controlling equations are as follows

$$S_{rr,r} + r^{-1}S_{r\theta,\theta} + r^{-1}(S_{rr} - S_{\theta\theta}) - p_s \left[u_{r,rr} + \frac{u_{r,r}}{r} - \frac{u_r}{r^2} + \frac{u_{r,\theta\theta}}{r^2} \right] = \rho(1 - \mathfrak{R}^2 \nabla_1^2) u_{r,tt} \quad (1)$$

$$S_{r\theta,r} + r^{-1}S_{\theta\theta,\theta} + 2r^{-1}S_{r\theta} - p_s \left[u_{\theta,rr} + \frac{u_{\theta,r}}{r} - \frac{u_\theta}{r^2} + \frac{u_{\theta,\theta\theta}}{r^2} \right] = \rho(1 - \mathfrak{R}^2 \nabla_1^2) u_{\theta,tt} \quad (2)$$

where $S_{rr}, S_{r\theta}, S_{\theta\theta}$ the stress modulli and ρ indicates mass density, $\mathfrak{R} = e_0 a$ where e_0 is a nonlocal parameter, a denotes the internal characteristics length and p_s denotes the hydro static factor.

The electric conduction equation of the piezoelectric plate is given by (Zenkour 2012)

$$\mathfrak{N}_{r,r} + r^{-1}\mathfrak{N}_r + r^{-1}\mathfrak{N}_{\theta,\theta} = 0 \quad (3)$$

The moisture diffusion is (Vinyas *et al.* 2018)

$$\varpi \theta_{r,r} + \varpi r^{-1}\theta_r + \varpi r^{-1}\theta_{\theta,\theta} = 0 \quad (4)$$

The thermal conductivity is given by

$$K \left[(T_{,rr} + r^{-1}T_{,r} + r^{-2}T_{,\theta\theta}) + \tau_T \frac{\partial}{\partial t} (T_{,rr} + r^{-1}T_{,r} + r^{-2}T_{,\theta\theta}) \right] - \rho C_v (1 - \mathfrak{R}^2 \nabla_1^2) (T_{,t} + \tau_q T_{,tt}) + \beta^* T_0 \nabla^2 \left[\frac{\partial}{\partial t} (u_{r,r} + r^{-1}(u_{\theta,\theta} + u_r)) + \tau_q \frac{\partial^2}{\partial t^2} (u_{r,r} + r^{-1}(u_{\theta,\theta} + u_r)) \right] = 0 \quad (5)$$

$$S_{rr} = (\lambda + 2\mu)e_{rr} + \lambda e_{\theta\theta} - \beta T - \mathfrak{I}C \quad (6)$$

$$S_{r\theta} = 2\mu e_{r\theta} \quad (7)$$

$$S_{\theta\theta} = \lambda e_{rr} + (\lambda + 2\mu)e_{\theta\theta} - \beta T - \mathfrak{I}C \quad (8)$$

$$\mathfrak{N}_r = \varepsilon_{11} E_r \quad (9)$$

$$\mathfrak{N}_\theta = \varepsilon_{11} E_\theta \quad (10)$$

$$\Theta_r = \eta_{11} C_r \quad (11)$$

$$\Theta_\theta = \eta_{11} C_\theta \quad (12)$$

$$\beta^* = \beta \left(1 + \beta_0 \frac{\partial}{\partial t} \right); \beta_0 = \frac{(3\lambda\alpha_0 + 2\mu\alpha_1)\alpha_T}{\beta}; \beta = (3\lambda + 2\mu)\alpha_T \quad (13)$$

here the strain is $e_{rr}, e_{r\theta}, e_{\theta\theta}$ and T is the temperature, λ, μ indicates the Lamé's parameter, C_v, β and K denotes the specific heat capacity, thermal capacity and the thermal conductivity, respectively in which α_0, α_1 and α_T is the thermal expansion coefficients. The Eq. (3) contains the electric components E_r, E_θ of the plate. In Eq. (4) ϖ indicates the moisture concentration with the components Θ_r, Θ_θ along with the moisture expansion η_{11} . In (5), T_0 is the reference temperature and τ_T, τ_q represent the phase lags of the temperature gradient and the heat flux.

The strain components corresponding to the polar coordinates (r, θ) are given by

$$e_{rr} = u_{r,r}; e_{r\theta} = 1/2 (u_{\theta,r} - r^{-1}(u_\theta - u_{r,\theta})); e_{\theta\theta} = r^{-1}(u_r + u_{\theta,\theta}) \quad (14)$$

The electric moduli is taken as

$$E_r = -E_{,r}; E_\theta = -r^{-1}E_{,\theta} \quad (15)$$

And the moisture diffusion Eq. (4) is compared typically in a way to the electric field and the diffusivity in the radial and circumferential directions are

$$C_r = -C_{,r}; C_\theta = -r^{-1}C_{,\theta} \quad (16)$$

The stress equation of motion is given by

$$S_{rr} = (\lambda + 2\mu)u_{r,r} + \lambda r^{-1}(u_r + u_{\theta,\theta}) - \beta T - \mathfrak{I}C \quad (17)$$

$$S_{\theta\theta} = \lambda u_{r,r} + (\lambda + 2\mu)r^{-1}(u_r + u_{\theta,\theta}) - \beta T - \mathfrak{I}C \quad (18)$$

$$S_{r\theta} = \mu (u_{\theta,r} - r^{-1}(u_\theta - u_{r,\theta})) \quad (19)$$

$$\mathfrak{I}_r = -\varepsilon_{11} E_{,r} \quad (20)$$

$$\mathfrak{I}_\theta = -r^{-1}\varepsilon_{11} E_{,\theta} \quad (21)$$

$$C_r = -\eta_{11} C_{,r} \quad (22)$$

$$C_\theta = -r^{-1}\eta_{11} C_{,\theta} \quad (23)$$

proposed material constants in nonhomogeneous form

$$\begin{aligned} \lambda &= \lambda r^{2m}, \mu = \mu r^{2m}, \varepsilon_{11} = \varepsilon_{11} r^{2m}, \varepsilon_{22} = \varepsilon_{22} r^{2m}, \rho = \rho(1 - \mathfrak{R}^2 \nabla_1^2) r^{2m}, \beta = \beta r^{2m}, \\ K &= K r^{2m}, \varpi = \varpi r^{2m}, p_s = p_s r^{2m}, \eta_{11} = \eta_{11} r^{2m} \end{aligned} \quad (24)$$

By the assumption of Eq. (24) for the non-homogeneous material in Eqs. (17)-(23) and then from Eqs. (1)-(5)

$$\begin{aligned} &(\lambda + 2\mu - p_s)(u_{r,rr} + r^{-1}u_{r,r} - r^{-2}u_r) + r^{-1}(\lambda + 2\mu)u_{\theta,r\theta} \\ &+ (\mu - p_s)r^{-2}u_{r,\theta\theta} - r^{-2}(\lambda + 2m\lambda - 3\mu)u_{\theta,\theta} + 2mr^{-1} \left(\begin{aligned} &(\lambda + 2\mu)u_r \\ &+ \lambda r^{-1}u_r - \beta T - \mathfrak{I}C \end{aligned} \right) \\ &\quad - \beta T_{,r} - \mathfrak{I}C_{,r} = \rho(1 - \mathfrak{R}^2 \nabla_1^2)u_{r,tt} \end{aligned} \quad (25)$$

$$\begin{aligned} &(\mu - p_s)(u_{\theta,rr} + r^{-1}u_{\theta,r} - r^{-2}u_\theta) + r^{-2}(\lambda + 2\mu - p_s)u_{\theta,\theta\theta} + r^{-2}(\lambda + 2m\mu + 3\mu)u_{r,\theta} \\ &+ 2m\mu r^{-1}(u_{\theta,r} - r^{-1}u_\theta) + (\lambda + \mu)r^{-1}u_{r,r\theta} - r^{-1}\beta T_{,\theta} - r^{-1}\mathfrak{I}C_{,\theta} = \rho(1 - \mathfrak{R}^2 \nabla_1^2)u_{\theta,tt} \end{aligned} \quad (26)$$

$$\varepsilon_{11}(\mathfrak{I}_{,rr} + r^{-1}\mathfrak{I}_{,r} + r^{-2}\mathfrak{I}_{,\theta\theta}) + 2mr^{-1}\varepsilon_{11}\mathfrak{I}_{,r} = 0 \quad (27)$$

$$\eta_{11}(C_{,rr} + r^{-1}C_{,r} + r^{-2}C_{,\theta\theta}) + 2mr^{-1}\eta_{11}C_{,r} = 0 \quad (28)$$

$$\begin{aligned} K \left[(T_{,rr} + r^{-1}T_{,r} + r^{-2}T_{,\theta\theta}) + \tau_T \frac{\partial}{\partial t} (T_{,rr} + r^{-1}T_{,r} + r^{-2}T_{,\theta\theta}) \right] - \rho C_v (1 - \mathfrak{R}^2 \nabla_1^2) (T_{,t} + \\ \tau_q T_{,tt}) + \beta T_0 \nabla^2 \left[\frac{\partial}{\partial t} (u_{r,r} + r^{-1}(u_{\theta,\theta} + u_r)) + \tau_q \frac{\partial^2}{\partial t^2} (u_{r,r} + r^{-1}(u_{\theta,\theta} + u_r)) \right] = 0 \end{aligned} \quad (29)$$

3. Solution of the problem

The Eqs. (25)-(29) are processed using the following relations Nagaya (1981)

$$u_r(r, \theta, t) = \sum_{n=0}^{\infty} \varepsilon_n \left[(r^{-1}\psi_{n,\theta} - \varphi_{n,r}) + (r^{-1}\bar{\psi}_{n,\theta} - \bar{\varphi}_{n,r}) \right] e^{i\omega t} \quad (30)$$

$$u_\theta(r, \theta, t) = \sum_{n=0}^{\infty} \varepsilon_n \left[(r^{-1}\varphi_{n,\theta} - \psi_{n,r}) + (r^{-1}\bar{\varphi}_{n,\theta} - \bar{\psi}_{n,r}) \right] e^{i\omega t} \quad (31)$$

$$E(r, \theta, t) = \sum_{n=0}^{\infty} \varepsilon_n (E_n + \bar{E}_n) e^{i\omega t} \quad (32)$$

$$C(r, \theta, t) = (\lambda + 2\mu/\beta a^2) \sum_{n=0}^{\infty} \varepsilon_n (C_n + \bar{C}_n) e^{i\omega t} \quad (33)$$

$$T(r, \theta) = (\lambda + 2\mu/\beta a^2) \sum_{n=0}^{\infty} \varepsilon_n (T_n + \bar{T}_n) e^{i\omega t} \quad (34)$$

where $\varepsilon_n = 1/2$ for $n = 0$ and $\varepsilon_n = 1$ for $n \geq 1$. To remove the complexity in above equations, we set up the dimensionless parameters as follows

$$\begin{aligned} &(\lambda + 2\mu - p_s)\nabla^2 \varphi_n + 2mr^{-1}(\lambda + 2\mu)\varphi_{n,r} - \rho(1 - \mathfrak{R}^2 \nabla_1^2)\omega^2 \varphi_n + \left(\frac{\lambda + 2\mu}{a^2} \right) T_n \\ &\quad + \mathfrak{I} \left(\frac{\lambda + 2\mu}{a^2 \varpi} \right) C_n = 0 \end{aligned} \quad (35)$$

$$(\mu - p_s)\nabla^2 \psi_n + 2mr^{-1}\mu\psi_{n,r} + \rho(1 - \mathfrak{R}^2 \nabla_1^2)\omega^2 \psi_n - \left(\frac{\lambda + 2\mu}{a^2} \right) T_n - \mathfrak{I} \left(\frac{\lambda + 2\mu}{a^2 \varpi} \right) C_n = 0 \quad (36)$$

$$\varepsilon_{11}\nabla^2 E_n + 2mr^{-1}\varepsilon_{11}E_{n,r} = 0 \quad (37)$$

$$\eta_{11}(\lambda + 2\mu/a^2\varpi)(\nabla^2 C_n + 2mr^{-1}C_{n,r}) = 0 \quad (38)$$

$$K \left[\begin{array}{l} \left(\frac{\lambda + 2\mu}{a^2\beta} \right) \\ (\nabla^2 T_n + \tau_T(i\omega)\nabla^2 T_n) \end{array} \right] - \rho(1 - \mathfrak{R}^2 \nabla_1^2) C_v \left[\begin{array}{l} \left(\frac{\lambda + 2\mu}{a^2\beta} \right) \left((i\omega T_n + T_{n,t}) \right. \\ \left. + \tau_q(-\omega^2 T_n + 2i\omega T_{n,t} + T_{n,tt}) \right) \end{array} \right] \\ + \beta^* T_0 \nabla^2 [i\omega(1 + \tau_q)(\psi_n + \varphi_n)] = 0 \quad (39)$$

Where

$$\nabla^2 = \frac{\partial^2}{\partial r^2} + \frac{1}{r} \frac{\partial}{\partial r} + \frac{1}{r^2} \frac{\partial^2}{\partial \theta^2} \quad (40)$$

We considered the time harmonic vibrations as

$$\begin{aligned} \varphi_n(r, \theta, t) &= r^{-m} \varphi_n(r) \cos n \theta e^{i\omega t} \\ \psi_n(r, \theta, t) &= r^{-m} \psi_n(r) \cos n \theta e^{i\omega t} \\ E_n(r, \theta, t) &= r^{-m} E_n(r) \cos n \theta e^{i\omega t} \\ C_n(r, \theta, t) &= r^{-m} C_n(r) \cos n \theta e^{i\omega t} \\ T_n(r, \theta, t) &= r^{-m} T_n(r) \cos n \theta e^{i\omega t} \end{aligned} \quad (41)$$

Using the set of Eq. (41) in Eqs. (35)-(39), we arrived as

$$\begin{aligned} \varphi_n''(r) + r^{-1} \varphi_n'(r) \left(\begin{array}{l} 1 - \frac{r^{-1}m(1+r)}{(\lambda+2\mu-p_s)} \\ + \frac{2m(\lambda+2\mu)}{\lambda+2\mu-p_s} \end{array} \right) + r^{-2} \varphi_n(r) \left[\frac{(m^2-2m-n^2)}{r^2} - \frac{(2m^2(\lambda+2\mu)-\rho(1-\mathfrak{R}^2 \nabla_1^2)\omega^2)r^2}{\lambda+2\mu-p_s} \right] \\ + \beta \frac{\lambda+2\mu}{a^2} T_n(r) + \frac{\mathfrak{I}(\lambda+2\mu)}{a^2\varpi} C_n(r) = 0 \end{aligned} \quad (42)$$

$$\varphi_n''(r) + r^{-1} \varphi_n'(r)(1 - g_1^2 + g_2^2) + r^{-2} \varphi_n(r)(g_3^2 - g_2^2 - \Omega^2) + g_4^2 \beta T_n(r) + \frac{g_4^2}{\varpi} \mathfrak{I} C_n(r) = 0 \quad (43)$$

$$\varphi_n''(r) + r^{-1} \varphi_n'(r) + r^{-2} \varphi_n(r)(n^2 r^2 - \beta^2) = 0 \quad (44)$$

where

$$n = \frac{\rho(1 - \mathfrak{R}^2)\omega^2}{\lambda + 2\mu - p_s}, \beta = \frac{(m^2 - 2m - n^2)}{\lambda + 2\mu - p_s}$$

The solution of Eq. (44) is given by the Bessel function as

$$\varphi_n(r) = (P_{1n} J_\beta(Nr) + P'_{1n} Y_\beta(Nr)) \cos n \theta \quad (45)$$

$$\begin{aligned} \psi_n''(r) + r^{-1} \psi_n'(r) \left(\frac{r^{-1}m(1+r)}{(\mu-p_s)} + \frac{2m\mu}{\mu-p_s} \right) + r^{-2} \psi_n(r) \left[\frac{(m^2-2m-n^2)}{r^2} + \frac{(2m^2\mu-\rho(1-\mathfrak{R}^2)\omega^2)r^2}{(\mu-p_s)} \right] \\ + \beta \frac{\lambda+2\mu}{a^2} T_n(r) - \frac{\mathfrak{I}(\lambda+2\mu)}{a^2\varpi} C_n(r) = 0 \end{aligned} \quad (46)$$

$$\psi_n''(r) + r^{-1} \psi_n'(r)(1 - g_5^2 + g_6^2) + r^{-2} \psi_n(r)(g_3^2 - g_7^2 - \Omega_1^2) - g_8^2 \beta T_n(r) - \frac{g_8^2}{\varpi} \mathfrak{I} C_n(r) = 0 \quad (47)$$

$$\psi_n''(r) + r^{-1} \psi_n'(r) + r^{-2} \psi_n(r)(\wp^2 r^2 - \delta^2) = 0 \quad (48)$$

where

Table 3 Comparison on non-dimensional frequencies for various aspect ratios of polygonal plates with ICOC boundary ($a/b=1.2, \Delta c=0.0, \mathfrak{R} = 0 \& \Delta T=43$)

a/b	Mode	Triangle		Square		Pentagon		Hexagon	
		Nagaya (1980)	Author						
0.1	L1	4.148	4.146	4.850	4.849	4.995	4.995	5.061	5.061
	L2	4.392	4.393	4.997	4.997	5.132	5.132	5.163	5.162
	L3	4.547	4.551	5.889	5.886	5.627	5.626	5.784	5.783
0.15	L1	4.269	4.267	5.128	5.127	5.297	5.296	5.367	5.365
	L2	4.510	4.511	5.271	5.272	5.419	5.418	5.449	5.446
	L3	4.769	4.765	6.069	6.068	5.782	5.784	5.951	5.945
0.2	L1	4.413	4.412	5.431	5.431	5.636	5.636	5.712	5.712
	L2	4.622	4.613	5.573	5.572	5.742	5.741	5.771	5.772
	L3	4.924	4.924	6.315	6.316	5.995	5.996	6.180	6.181
0.25	L1	4.474	4.573	5.757	5.756	6.018	6.017	6.103	6.103
	L2	4.739	4.738	5.910	5.911	6.106	6.104	6.138	6.136
	L3	5.019	5.016	6.627	6.627	6.264	6.265	6.470	6.471

by Nagaya (1980) has been adopted as

$$(S_{xx})_j = (S_{xy})_j = (\mathfrak{I}_r)_j = (C_r)_j = (T_r)_j = 0 \tag{60}$$

The normal coordinate x and the tangential coordinate y is depicted as in Fig. 2. The transformed equations are discussed as follows along nonlinear surface of the boundary

$$u_r = u_r \cos(\theta - \gamma_i) - u_\theta \sin(\theta - \gamma_i) \tag{61}$$

$$u_\theta = u_\theta \cos(\theta - \gamma_i) + u_r \sin(\theta - \gamma_i) \tag{62}$$

$$\frac{\partial r}{\partial x_i} = \cos(\theta - \gamma_i), \frac{\partial \theta}{\partial x_i} = -r^{-1} \sin(\theta - \gamma_i) \tag{63}$$

$$\frac{\partial r}{\partial y_i} = \sin(\theta - \gamma_i), \frac{\partial \theta}{\partial y_i} = r^{-1} \cos(\theta - \gamma_i) \tag{64}$$

Using the above Eqs. (61)-(64), the elasticity equations becomes

$$S_{xx} = ((\lambda + 2\mu) \cos^2(\theta - \gamma_i) + \lambda \sin^2(\theta - \gamma_i))u_{r,r} + r^{-1} \left(\begin{matrix} (\lambda + 2\mu) \sin^2(\theta - \gamma_i) \\ + \lambda \cos^2(\theta - \gamma_i) \end{matrix} \right) (u_r + u_{\theta,\theta}) + \frac{u_\theta}{2} (r^{-1}(u_\theta - u_{r,\theta}) - u_{\theta,r}) \sin 2(\theta - \gamma_i) - \beta T - \frac{\mathfrak{I}}{\omega} C = 0 \tag{65}$$

$$S_{xy} = \mu \left(\begin{matrix} (u_{r,r} - r^{-1}u_{\theta,\theta} - r^{-1}u_r) \sin 2(\theta - \gamma_i) \\ \cos 2(\theta - \gamma_i) \end{matrix} + (r^{-1}u_{r,\theta} + u_{\theta,r} - r^{-1}u_\theta) \right) = 0 \tag{66}$$

$$E_x = -\varepsilon_{11}E_r = 0 \tag{67}$$

$$C_x = -\eta_{11}C_r = 0 \tag{68}$$

Incorporating the obtained solution Eq. (60), we get

$$\begin{aligned} \left[(Z_{xx})_j + (\bar{Z}_{xx})_j \right] e^{i\omega t} &= 0 \\ \left[(Z_{xy})_j + (\bar{Z}_{xy})_j \right] e^{i\omega t} &= 0 \\ \left[(E_x)_j + (\bar{E}_x)_j \right] e^{i\omega t} &= 0 \\ \left[(C_x)_j + (\bar{C}_x)_j \right] e^{i\omega t} &= 0 \\ \left[(T_x)_j + (\bar{T}_x)_j \right] e^{i\omega t} &= 0 \end{aligned} \tag{69}$$

where

$$\begin{aligned} Z_{xx} &= 0.5(P_{10}u_0^1 + P_{20}u_0^2 + P_{30}u_0^3) + \sum_{n=1}^{\infty}(P_{1n}u_n^1 + P_{2n}u_n^2 + P_{3n}u_n^3 + P_{4n}u_n^4) \\ Z_{xy} &= 0.5(P_{10}v_0^1 + P_{20}v_0^2 + P_{30}v_0^3) + \sum_{n=1}^{\infty}(P_{1n}v_n^1 + P_{2n}v_n^2 + P_{3n}v_n^3 + P_{4n}v_n^4) \\ E_x &= 0.5(P_{10}w_0^1 + P_{20}w_0^2 + P_{30}w_0^3) + \sum_{n=1}^{\infty}(P_{1n}w_n^1 + P_{2n}w_n^2 + P_{3n}w_n^3 + P_{4n}w_n^4) \\ C_x &= 0.5(P_{10}x_0^1 + P_{20}x_0^2 + P_{30}x_0^3) + \sum_{n=1}^{\infty}(P_{1n}x_n^1 + P_{2n}x_n^2 + P_{3n}x_n^3 + P_{4n}x_n^4) \\ T_x &= 0.5(P_{10}y_0^1 + P_{20}y_0^2 + P_{30}y_0^3) + \sum_{n=1}^{\infty}(P_{1n}y_n^1 + P_{2n}y_n^2 + P_{3n}y_n^3 + P_{4n}y_n^4) \end{aligned} \tag{70}$$

For anti-symmetric mode

$$\begin{aligned} \bar{Z}_{xx} &= 0.5(\bar{P}_{40}\bar{u}\bar{e}_0^4) + \sum_{n=1}^{\infty}(\bar{P}_{1n}\bar{u}_n^1 + \bar{P}_{2n}\bar{u}_n^2 + \bar{P}_{3n}\bar{u}_n^3 + \bar{P}_{4n}\bar{u}_n^4) \\ \bar{Z}_{xy} &= 0.5(\bar{P}_{40}\bar{v}_0^4) + \sum_{n=1}^{\infty}(\bar{P}_{1n}\bar{v}_n^1 + \bar{P}_{2n}\bar{v}_n^2 + \bar{P}_{3n}\bar{v}_n^3 + \bar{P}_{4n}\bar{v}_n^4) \\ \bar{E}_x &= 0.5(\bar{P}_{40}\bar{w}_0^4) + \sum_{n=1}^{\infty}(\bar{P}_{1n}\bar{w}_n^1 + \bar{P}_{2n}\bar{w}_n^2 + \bar{P}_{3n}\bar{w}_n^3 + \bar{P}_{4n}\bar{w}_n^4) \\ \bar{C}_x &= 0.5(\bar{P}_{40}\bar{x}_0^4) + \sum_{n=1}^{\infty}(\bar{P}_{1n}\bar{x}_n^1 + \bar{P}_{2n}\bar{x}_n^2 + \bar{P}_{3n}\bar{x}_n^3 + \bar{P}_{4n}\bar{x}_n^4) \\ \bar{T}_x &= 0.5(\bar{P}_{40}\bar{y}_0^4) + \sum_{n=1}^{\infty}(\bar{P}_{1n}\bar{y}_n^1 + \bar{P}_{2n}\bar{y}_n^2 + \bar{P}_{3n}\bar{y}_n^3 + \bar{P}_{4n}\bar{y}_n^4) \end{aligned} \tag{71}$$

Using the Fourier expansion collocation method to (60) along the boundary surfaces are expanded using Fourier double series. Hence the boundary conditions are obtained as,

For symmetric mode

$$\begin{aligned} \sum_{m=0}^{\infty} \varepsilon_m [U_{m0}^1 P_{10} + U_{m0}^2 P_{20} + \sum_{n=1}^{\infty} (U_{mn}^1 P_{1n} + U_{mn}^2 P_{2n} + U_{mn}^3 P_{3n})] \cos m\theta &= 0 \\ \sum_{m=0}^{\infty} [V_{m0}^1 P_{10} + V_{m0}^2 P_{20} + \sum_{n=1}^{\infty} (V_{mn}^1 P_{1n} + V_{mn}^2 P_{2n} + V_{mn}^3 P_{3n})] \sin m\theta &= 0 \\ \sum_{m=0}^{\infty} \varepsilon_m [W_{m0}^1 P_{10} + W_{m0}^2 P_{20} + \sum_{n=1}^{\infty} (W_{mn}^1 P_{1n} + W_{mn}^2 P_{2n} + W_{mn}^3 P_{3n})] \cos m\theta &= 0 \\ \sum_{m=0}^{\infty} \varepsilon_m [X_{m0}^1 P_{10} + X_{m0}^2 P_{20} + \sum_{n=1}^{\infty} (X_{mn}^1 P_{1n} + X_{mn}^2 P_{2n} + X_{mn}^3 P_{3n})] \cos m\theta &= 0 \\ \sum_{m=0}^{\infty} \varepsilon_m [Y_{m0}^1 P_{10} + Y_{m0}^2 P_{20} + \sum_{n=1}^{\infty} (Y_{mn}^1 P_{1n} + Y_{mn}^2 P_{2n} + Y_{mn}^3 P_{3n})] \cos m\theta &= 0 \end{aligned} \tag{72}$$

where

$$\begin{aligned} U_{mn}^j &= \frac{2\varepsilon_n}{\pi} \sum_{\ell=1}^S \int_{\theta_{i-1}}^{\theta} u_n^j(R_{\ell}, \theta) \cos m\theta d\theta \\ V_{mn}^j &= \frac{2\varepsilon_n}{\pi} \sum_{\ell=1}^S \int_{\theta_{i-1}}^{\theta} v_n^j(R_{\ell}, \theta) \sin m\theta d\theta \\ W_{mn}^j &= \frac{2\varepsilon_n}{\pi} \sum_{\ell=1}^S \int_{\theta_{i-1}}^{\theta} w_n^j(R_{\ell}, \theta) \cos m\theta d\theta \end{aligned}$$

$$\begin{aligned}
 X_{mn}^j &= \frac{2\varepsilon_n}{\pi} \sum_{\ell=1}^S \int_{\theta_{i-1}}^{\theta} x_n^j(R_\ell, \theta) \cos m \theta d\theta \\
 Y_{mn}^j &= \frac{2\varepsilon_n}{\pi} \sum_{\ell=1}^S \int_{\theta_{i-1}}^{\theta} y_n^j(R_\ell, \theta) \cos m \theta d\theta
 \end{aligned}
 \tag{73}$$

For the non trivial solution the determinants of the co efficient matrices $P_{iN} = 0$ and $\overline{P}_{iN} = 0$ the elements give the frequencies of the symmetric mode and anti-symmetric mode as in Eqs. (74) and (77) respectively.

$$\begin{vmatrix}
 U_{00}^1 & U_{00}^2 & U_{01}^1 & \dots & U_{0N}^1 & U_{01}^2 & \dots & U_{0N}^2 & U_{01}^3 & \dots & U_{0N}^3 \\
 \vdots & \vdots & \vdots & & \vdots & \vdots & & \vdots & \vdots & & \vdots \\
 U_{N0}^1 & U_{N0}^2 & U_{N1}^1 & \dots & U_{NN}^1 & U_{N1}^2 & \dots & U_{NN}^2 & U_{N1}^3 & \dots & U_{NN}^3 \\
 V_{00}^1 & V_{00}^2 & V_{01}^1 & \dots & V_{0N}^1 & V_{01}^2 & \dots & V_{0N}^2 & V_{01}^3 & \dots & V_{0N}^3 \\
 \vdots & \vdots & \vdots & & \vdots & \vdots & & \vdots & \vdots & & \vdots \\
 V_{N0}^1 & V_{N0}^2 & V_{N1}^1 & \dots & V_{NN}^1 & V_{N1}^2 & \dots & V_{NN}^2 & V_{N1}^3 & \dots & V_{NN}^3 \\
 W_{00}^1 & W_{00}^2 & W_{01}^1 & \dots & W_{0N}^1 & W_{01}^2 & \dots & W_{0N}^2 & W_{01}^3 & \dots & W_{0N}^3 \\
 \vdots & \vdots & \vdots & & \vdots & \vdots & & \vdots & \vdots & & \vdots \\
 W_{N0}^1 & W_{N0}^2 & W_{N1}^1 & \dots & W_{NN}^1 & W_{N1}^2 & \dots & W_{NN}^2 & W_{N1}^3 & \dots & W_{NN}^3 \\
 X_{00}^1 & X_{00}^2 & X_{01}^1 & \dots & X_{0N}^1 & X_{01}^2 & \dots & X_{0N}^2 & X_{01}^3 & \dots & X_{0N}^3 \\
 \vdots & \vdots & \vdots & & \vdots & \vdots & & \vdots & \vdots & & \vdots \\
 X_{N0}^1 & X_{N0}^2 & X_{N1}^1 & \dots & X_{NN}^1 & X_{N1}^2 & \dots & X_{NN}^2 & X_{N1}^3 & \dots & X_{NN}^3 \\
 Y_{00}^1 & Y_{00}^2 & Y_{01}^1 & \dots & Y_{0N}^1 & Y_{01}^2 & \dots & Y_{0N}^2 & Y_{01}^3 & \dots & Y_{0N}^3 \\
 \vdots & \vdots & \vdots & & \vdots & \vdots & & \vdots & \vdots & & \vdots \\
 Y_{N0}^1 & Y_{N0}^2 & Y_{N1}^1 & \dots & Y_{NN}^1 & Y_{N1}^2 & \dots & Y_{NN}^2 & Y_{N1}^3 & \dots & Y_{NN}^3
 \end{vmatrix} = 0 \tag{74}$$

For Anti symmetric mode

$$\begin{aligned}
 \sum_{m=0}^{\infty} [\overline{U}_{m0}^3 P_{30} + \sum_{n=1}^{\infty} (\overline{U}_{mn}^1 P_{1n} + \overline{U}_{mn}^2 P_{2n} + \overline{U}_{mn}^3 P_{3n})] \sin m \theta &= 0 \\
 \sum_{m=0}^{\infty} \varepsilon_m [\overline{V}_{m0}^3 P_{30} + \sum_{n=1}^{\infty} (\overline{V}_{mn}^1 P_{1n} + \overline{V}_{mn}^2 P_{2n} + \overline{V}_{mn}^3 P_{3n})] \cos m \theta &= 0 \\
 \sum_{m=0}^{\infty} [\overline{W}_{m0}^3 P_{30} + \sum_{n=1}^{\infty} (\overline{W}_{mn}^1 P_{1n} + \overline{W}_{mn}^2 P_{2n} + \overline{W}_{mn}^3 P_{3n})] \sin m \theta &= 0 \\
 \sum_{m=0}^{\infty} [\overline{X}_{m0}^3 P_{30} + \sum_{n=1}^{\infty} (\overline{X}_{mn}^1 P_{1n} + \overline{X}_{mn}^2 P_{2n} + \overline{X}_{mn}^3 P_{3n})] \sin m \theta &= 0 \\
 \sum_{m=0}^{\infty} [\overline{Y}_{m0}^3 P_{30} + \sum_{n=1}^{\infty} (\overline{Y}_{mn}^1 P_{1n} + \overline{Y}_{mn}^2 P_{2n} + \overline{Y}_{mn}^3 P_{3n})] \sin m \theta &= 0
 \end{aligned}
 \tag{75}$$

where

$$\begin{aligned}
 \overline{U}_{mn}^j &= \frac{2\varepsilon_n}{\pi} \sum_{\ell=1}^S \int_{\theta_{i-1}}^{\theta} \overline{u}_n^j(R_\ell, \theta) \sin m \theta d\theta \\
 \overline{V}_{mn}^j &= \frac{2\varepsilon_n}{\pi} \sum_{\ell=1}^S \int_{\theta_{i-1}}^{\theta} \overline{v}_n^j(R_\ell, \theta) \cos m \theta d\theta \\
 \overline{W}_{mn}^j &= \frac{2\varepsilon_n}{\pi} \sum_{\ell=1}^S \int_{\theta_{i-1}}^{\theta} \overline{w}_n^j(R_\ell, \theta) \sin m \theta d\theta \\
 \overline{X}_{mn}^j &= \frac{2\varepsilon_n}{\pi} \sum_{\ell=1}^S \int_{\theta_{i-1}}^{\theta} \overline{x}_n^j(R_\ell, \theta) \sin m \theta d\theta
 \end{aligned}$$

$$\bar{Y}_{mn}^j = \frac{2\varepsilon_n}{\pi} \sum_{\ell=1}^S \int_{\theta_{i-1}}^{\theta} \bar{y}_n^j(R_\ell, \theta) \sin m \theta d\theta \tag{76}$$

$$\begin{pmatrix} \bar{U}_{00}^1 & \bar{U}_{00}^2 & \bar{U}_{01}^1 & \dots & \bar{U}_{0N}^1 & \bar{U}_{01}^2 & \dots & \bar{U}_{0N}^2 & \bar{U}_{01}^3 & \dots & \bar{U}_{0N}^3 \\ \vdots & \vdots & \vdots & & \vdots & \vdots & & \vdots & \vdots & & \vdots \\ \bar{U}_{N0}^1 & \bar{U}_{N0}^2 & \bar{U}_{N1}^1 & \dots & \bar{U}_{NN}^1 & \bar{U}_{N1}^2 & \dots & \bar{U}_{NN}^2 & \bar{U}_{N1}^3 & \dots & \bar{U}_{NN}^3 \\ \bar{V}_{00}^1 & \bar{V}_{00}^2 & \bar{V}_{01}^1 & \dots & \bar{V}_{0N}^1 & \bar{V}_{01}^2 & \dots & \bar{V}_{0N}^2 & \bar{V}_{01}^3 & \dots & \bar{V}_{0N}^3 \\ \vdots & \vdots & \vdots & & \vdots & \vdots & & \vdots & \vdots & & \vdots \\ \bar{V}_{N0}^1 & \bar{V}_{N0}^2 & \bar{V}_{N1}^1 & \dots & \bar{V}_{NN}^1 & \bar{V}_{N1}^2 & \dots & \bar{V}_{NN}^2 & \bar{V}_{N1}^3 & \dots & \bar{V}_{NN}^3 \\ \bar{W}_{00}^1 & \bar{W}_{00}^2 & \bar{W}_{01}^1 & \dots & \bar{W}_{0N}^1 & \bar{W}_{01}^2 & \dots & \bar{W}_{0N}^2 & \bar{W}_{01}^3 & \dots & \bar{W}_{0N}^3 \\ \vdots & \vdots & \vdots & & \vdots & \vdots & & \vdots & \vdots & & \vdots \\ \bar{W}_{N0}^1 & \bar{W}_{N0}^2 & \bar{W}_{N1}^1 & \dots & \bar{W}_{NN}^1 & \bar{W}_{N1}^2 & \dots & \bar{W}_{NN}^2 & \bar{W}_{N1}^3 & \dots & \bar{W}_{NN}^3 \\ \bar{X}_{00}^1 & \bar{X}_{00}^2 & \bar{X}_{01}^1 & \dots & \bar{X}_{0N}^1 & \bar{X}_{01}^2 & \dots & \bar{X}_{0N}^2 & \bar{X}_{01}^3 & \dots & \bar{X}_{0N}^3 \\ \vdots & \vdots & \vdots & & \vdots & \vdots & & \vdots & \vdots & & \vdots \\ \bar{X}_{N0}^1 & \bar{X}_{N0}^2 & \bar{X}_{N1}^1 & \dots & \bar{X}_{NN}^1 & \bar{X}_{N1}^2 & \dots & \bar{X}_{NN}^2 & \bar{X}_{N1}^3 & \dots & \bar{X}_{NN}^3 \\ \bar{Y}_{00}^1 & \bar{Y}_{00}^2 & \bar{Y}_{01}^1 & \dots & \bar{Y}_{0N}^1 & \bar{Y}_{01}^2 & \dots & \bar{Y}_{0N}^2 & \bar{Y}_{01}^3 & \dots & \bar{Y}_{0N}^3 \\ \vdots & \vdots & \vdots & & \vdots & \vdots & & \vdots & \vdots & & \vdots \\ \bar{Y}_{N0}^1 & \bar{Y}_{N0}^2 & \bar{Y}_{N1}^1 & \dots & \bar{Y}_{NN}^1 & \bar{Y}_{N1}^2 & \dots & \bar{Y}_{NN}^2 & \bar{Y}_{N1}^3 & \dots & \bar{Y}_{NN}^3 \end{pmatrix} = 0 \tag{77}$$

5. Numerical results and discussion

For the authentication of analytical outputs, some simulations and computations are carried out over the physical constants of copper from Selvamani and Ponnusamy (2013b)

$$\begin{aligned} \nu &= 0.3, \rho = 8.96 \times 10^3 \text{ kg/m}^3, E = 2.139 \times 10^{11} \text{ N/m}^2, \lambda = 8.20 \times 10^{11} \text{ kg/ms}^2, \mu = \\ &4.20 \times 10^{10} \text{ kg/ms}^2, c_v = 9.1 \times \frac{10^{-2} \text{ m}^2}{\text{ks}^2}, K = 113 \times 10^{-2} \text{ kgm/ks}^2, T_0 = 23^\circ\text{C}, C_0 = \\ &0.3\text{wt}\% \text{H}_2\text{O}, m_{11} = -3612 \times 10^{-11} \text{ Ns/VC}, \varepsilon_{11} = 8.26 \times 10^{-11} \text{ C}^2\text{N}^{-1}\text{m}^2, \\ &\mu_{11} = -5 \times 10^{-6} \text{ Ns}^2/\text{C}^2 \end{aligned}$$

The geometry of poly plate is considered from Nagaya (1980) as

$$R_i/a = [\cos(\theta - \gamma_i)]^{-1}, R_i/b = [\cos(\theta - \gamma_i)]^{-1}, \gamma_i = \gamma_i.$$

Table 1 presents the comparative study between the numerical results of the non-dimensional frequency for the piezoelectric plate which is clamped inner and outer sides by (Nagaya 1974) and the current article in the absence of moisture, initial stress and nonlocal parameter. Results predict the reasonable agreement with the literature.

Figs. 3 and 4 illustrate the dispersion curves for the radial stress S_{rr} under the hydrostatical stress and nonlocal parameter $p_s = 0.0, p_s = 0.5$ and $\mathfrak{R} = 0, 0.03$ of various shapes such as triangle, square, pentagon and hexagon of the non-homogeneous piezoelectric plate for the different aspect ratio a/b . From these figures it is observed that the radial stress is increasing when the aspect ratio is increasing and also the stress in the radial direction is inflated for the hexagonal cross section comparing with the other cross sections. Also from the Fig. 4 it is observed that the

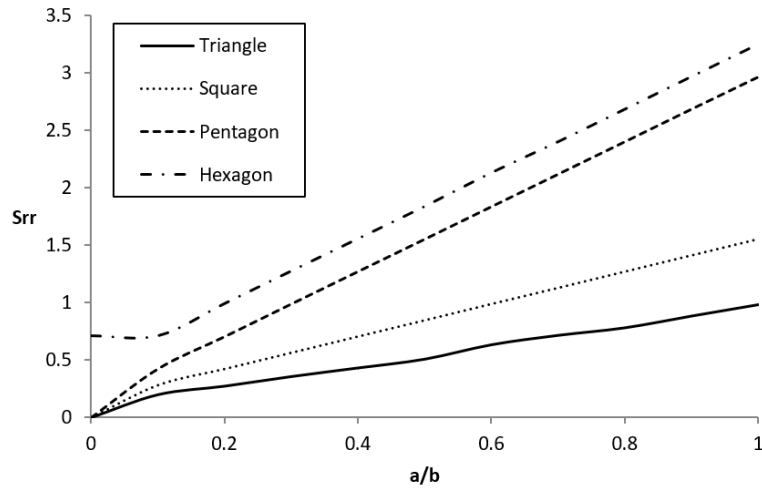


Fig. 3 Radial stress with aspect ratio a/b via $p_s = 0.0, \mathfrak{R} = 0 \& C = 0.0$

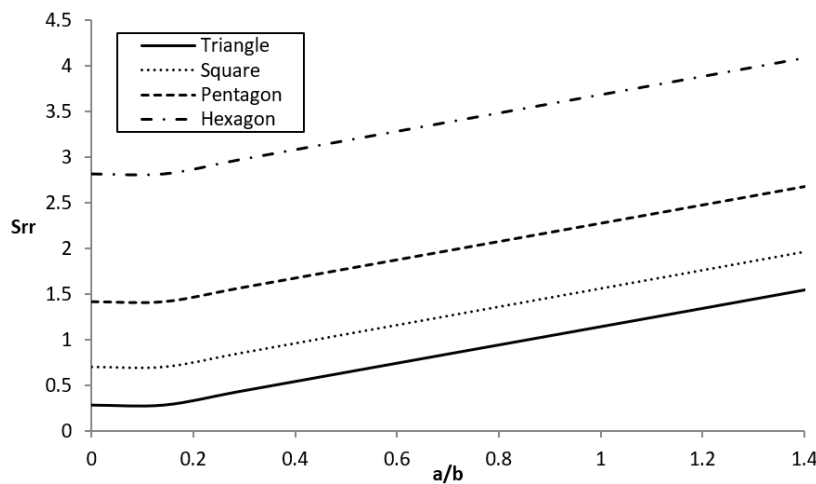


Fig. 4 Radial stress with aspect ratio a/b via $p_s = 0.5, \mathfrak{R} = 0.03 \& \Delta C = 0.5$

deviation of the radial stresses is more between the various shapes of the plate and significance of nonlocal parameter.

Figs. 5 and 6 illustrate the dispersion curves for the displacement u with aspect ratio a/b under $p_s = 0.0, \Delta C = 0.0, \mathfrak{R} = 0.0$ and $p_s = 0.5, \Delta C = 0.5, \mathfrak{R} = 0.03$ for the nonhomogeneous piezoelectric poly plate. When the aspect ratio increases the displacement decreases in the presence of zero moisture and initial stress in Fig. 5. But in Fig. 6, there is an increment in the amplitude of decaying displacement due to the large values of moisture, initial stress and nonlocal parameter. In these figures it is also observed that when the number of sides of cross section is more, then the displacement is decaying and falls to the minimum value deliberately. The hexagon cross sectional plate needs more displacement value when the aspect ratio is zero.

The temperature distribution of the various shapes of the plate at $p_s = 0, \Delta C = 0, \mathfrak{R} = 0$ and $p_s = 0.5, \Delta C = 0.5, \mathfrak{R} = 0.03$ are shown in Figs. 7 and 8. It is noticed that the temperature

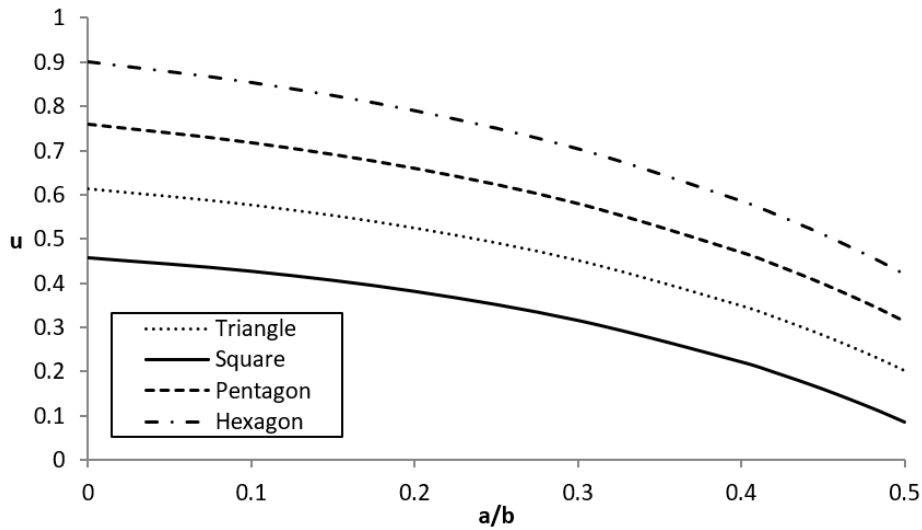


Fig. 5 Displacement with aspect ratio a/b via $p_s = 0.0, \mathfrak{R} = 0 \& \Delta C = 0.0$

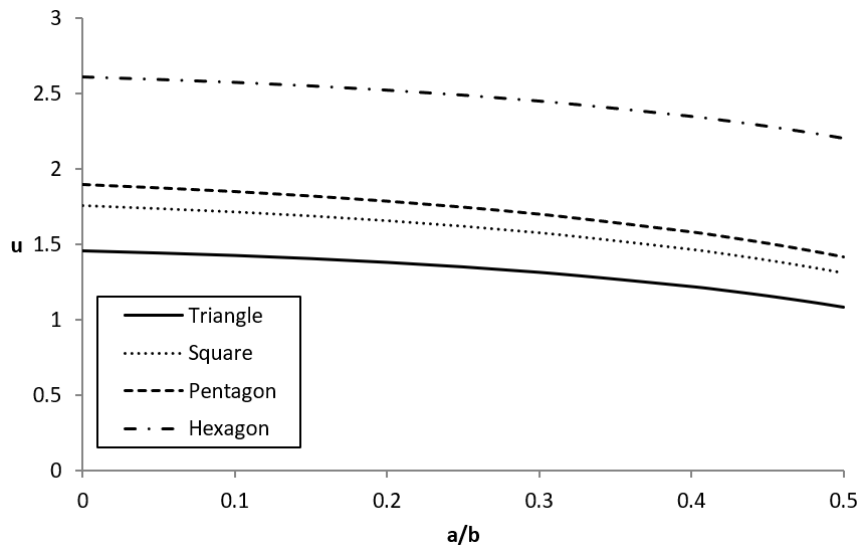


Fig. 6 Displacement with aspect ratio a/b via $p_s = 0.5, \mathfrak{R} = 0.03 \& \Delta C = 0.5$

distribution decays between 0 and 2 and gives smooth values where the aspect ratio greater than 2. Moreover the hexagonal plate is provides smooth temperature distribution even it requires higher amplitude than the other shapes and also the effect of moisture, initial stress and nonlocal parameter is noticed due to the dispersion among the modes in Fig. 8.

The electrical displacement of the various shapes of the poly plate is presented via $p_s = 0, \mathfrak{R} = 0$ and $p_s = 0.5, \mathfrak{R} = 0.03$ in Figs. 9 and 10.

Here also we are experiencing the decreasing trend in electric displacement as aspect ratio grows via moisture and initial stress. These also indicates that the hexagon shape plate needs highest input than the other shapes and the distribution decays when the aspect ratio is increasing.

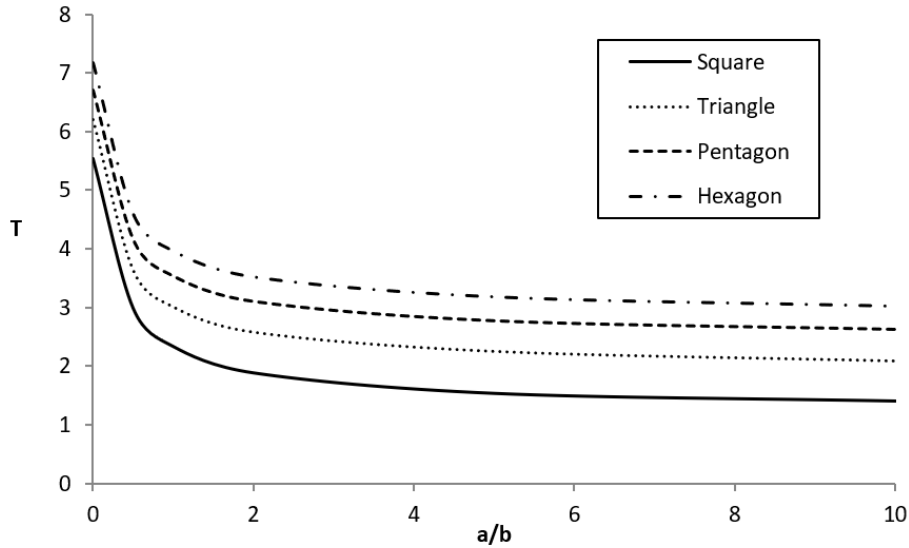


Fig. 7 Temperature distribution with aspect ratio a/b via $p_s = 0.0, \mathfrak{R} = 0 \& \Delta C = 0$

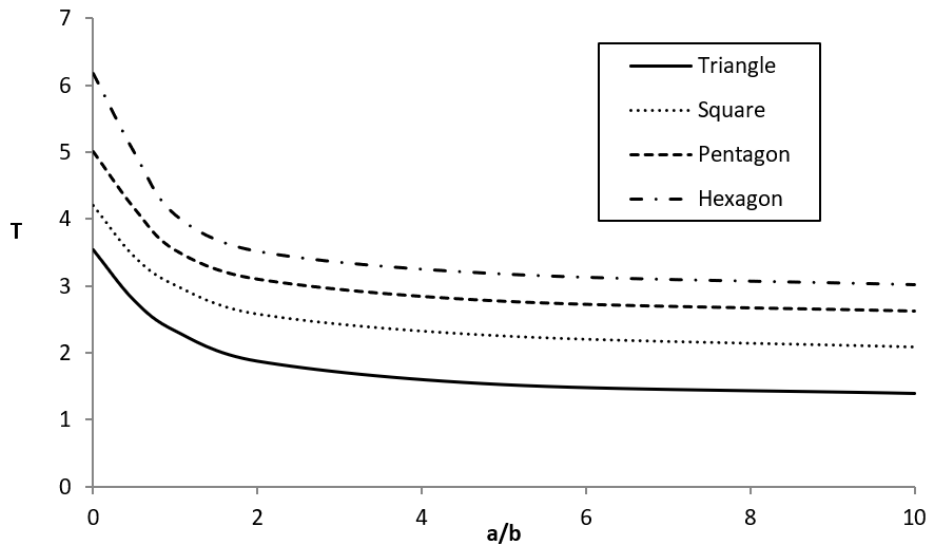


Fig. 8 Temperature distribution with aspect ratio a/b via $p_s = 0.5, \mathfrak{R} = 0.03 \& \Delta C = 0.5$

Particularly, when the pre-stress factor is 0.5 the square and pentagon shape plates give the similar distribution while the aspect ratio is 0.5.

Figs. 11 and 12 display the moisture distribution of the various shapes of the poly plate via $p_s = 0, \mathfrak{R} = 0$ and $p_s = 0.5, \mathfrak{R} = 0.03$. It is noticed that the moisture distribution decays steadily as aspect ratio increases and damped in higher aspect ratio with amplified values of p_s and \mathfrak{R} . In this graph, it clear that, hexagonal shape plates decays quickly than other plates.

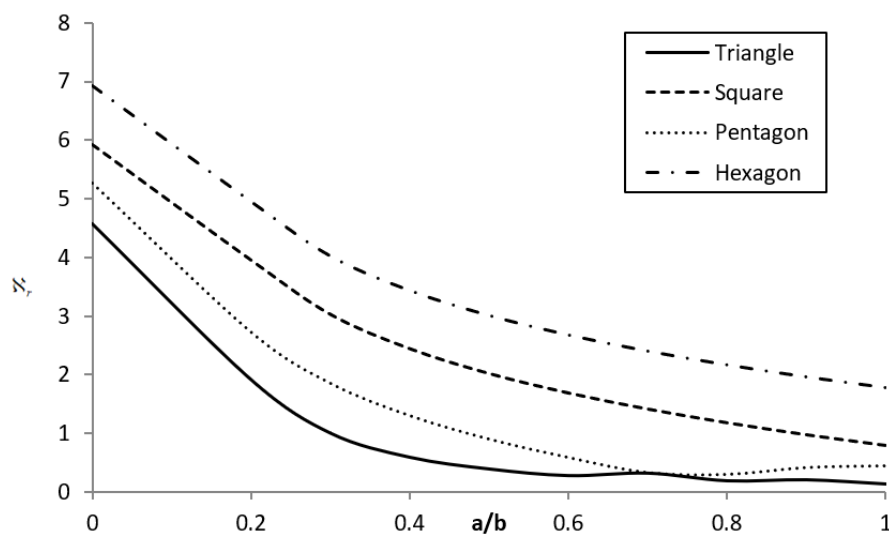


Fig. 9 Electrical distribution with aspect ratio a/b via $p_s = 0.0$ & $\mathcal{R} = 0$

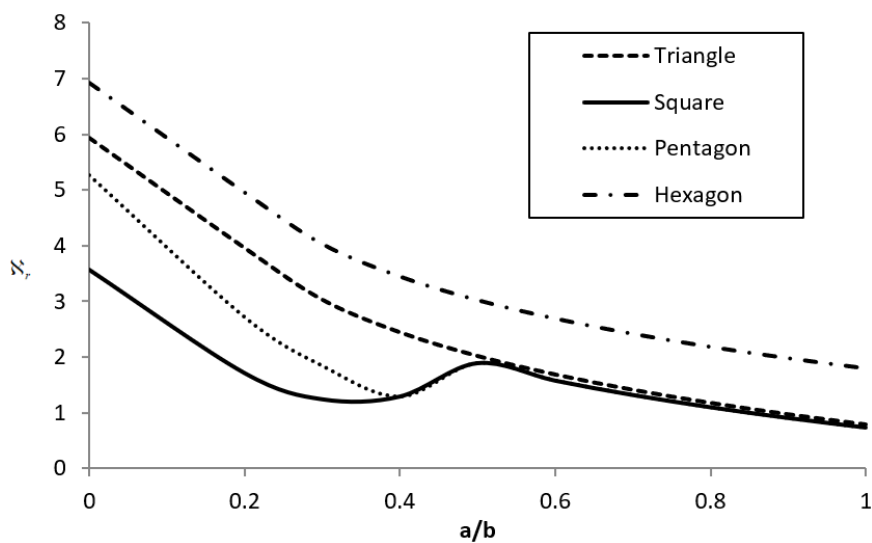


Fig. 10 Electrical distribution with aspect ratio a/b via $p_s = 0.5$ & $\mathcal{R} = 0.03$

6. Conclusions

In this paper, the effects of humidity and initial stress on the vibrations of a nonlocal, non-homogeneous prestressed thermo piezoelectric plate have been formulated and discussed using the linear elasticity theory. This study shows

- The larger aspect ratio leads to the larger stress values of poly plates with moisture and the initial stress effect.
- The mechanical displacement attains higher amplitude at a lower aspect ratio via moisture and initial stress variation.

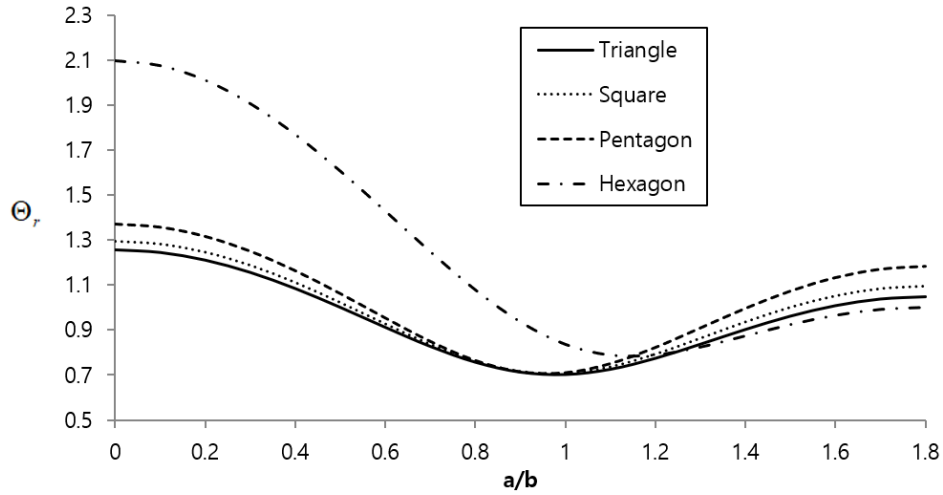


Fig. 11 Moisture distribution with aspect ratio a/b via $p_s = 0$ & $\mathcal{R} = 0.0$

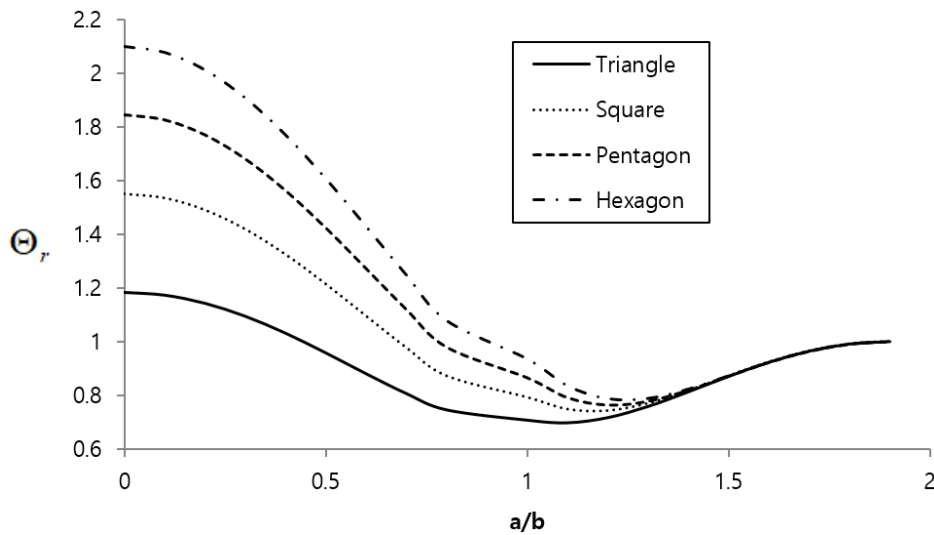


Fig. 12 Moisture distribution with aspect ratio a/b via $p_s = 0.5$ & $\mathcal{R} = 0.03$

- The increase in aspect ratio results in a decrease in temperature and electrical distribution due to moisture and the initial stress change.
- The elastic nonlocal parameter significantly affects the output of the physical variants.
- The inflated magnitude has been observed in hexagonal plates in all physical quantities.
- On nonlinear boundaries, the Fourier expansion collocation method achieves better performance.
- The results of this study might have useful applications in the field of smart and novel materials as well as in structures with nonlinear boundaries.

References

- Abbas, I.A., Abdalla, A. and Sapor, H. (2022), "Nonlocal heat conduction approach in biological tissue generated by laser irradiation", *Adv. Mater. Res.*, **11**(2), 111-120. <https://doi.org/10.12989/amr.2022.11.2.111>.
- Adams, D.F. and Keith Miller, A. (1977), "Hygrothermal microstress in a unidirectional composite exhibiting inelastic material behavior". *J. Compos. Mater.*, **11**, 285-299. <https://doi.org/10.1177/002199837701100304>.
- Al-Osta, M.A., Saidi, H., Tounsi, A., Al-Dulaijan, S.U., Al-Zahrani, M.M., Sharif, A. and Tounsi, A. (2021), "Influence of porosity on the hygro-thermo-mechanical bending response of an AFG ceramic-metal plates using an integral plate model", *Smart Struct. Syst.*, **28**(4), 499-513. <http://doi.org/10.12989/sss.2021.28.4.499>.
- Amar, L.H.H., Bourada, F., Bousahla, A.A., Tounsi, A., Benrahou, K.H., Albalawi, H. and Tounsi, A. (2023), "Buckling analysis of FG plates via 2D and quasi-3D refined shear deformation theories", *Struct. Eng. Mech.*, **85**(6), 765-780. <https://doi.org/10.12989/sem.2023.85.6.765>.
- Bakoura, A., Djedid, I.K., Bourada, F., Bousahla, A.A., Mahmoud, S.R., Tounsi, A., ... & Alnujaie, A. (2022), "A mechanical behavior of composite plates using a simple three variable refined plate theory", *Struct. Eng. Mech.*, **83**(5), 617-625. <https://doi.org/10.12989/sem.2022.83.5.617>.
- Belbachir, N., Bourada, F., Bousahla, A.A., Tounsi, A., Al-Osta, M.A., Ghazwani, M.H., ... & Tounsi, A. (2023), "A refined quasi-3D theory for stability and dynamic investigation of cross-ply laminated composite plates on Winkler-Pasternak foundation", *Struct. Eng. Mech.*, **85**(4), 433-443. <https://doi.org/10.12989/sem.2023.85.4.433>.
- Benedjadi, M., Aldosari, S.M., Chikh, A., Kaci, A., Bousahla, A.A., Bourada, F., ... & Tounsi, A. (2023), "Visco-elastic foundation effect on buckling response of exponentially graded sandwich plates under various boundary conditions", *Geomech. Eng.*, **32**(2), 159-177. <https://doi.org/10.12989/gae.2023.32.2.159>.
- Bin, W., Jiangong, J. and Cunfu, H. (2008), "Wave propagation in non-homogeneous magneto-electro-elastic plates", *J. Sound Vib.*, **317**, 250-264. <http://doi.org/10.1016/j.jsv.2008.03.008>.
- Bot, I.K., Bousahla, A.A., Zemri, A., Sekkal, M., Kaci, A., Bourada, F., ... & Mahmoud, S.R. (2022), "Effects of Pasternak foundation on the bending behavior of FG porous plates in hygrothermal environment", *Steel Compos. Struct.*, **43**(6), 821-837. <https://doi.org/10.12989/scs.2022.43.6.821>.
- Bouafia, K., Selim, M.M., Bourada, F., Bousahla, A.A., Bourada, M., Tounsi, A., ... & Tounsi, A. (2021), "Bending and free vibration characteristics of various compositions of FG plates on elastic foundation via quasi 3D HSDT model", *Steel Compos. Struct.*, **41**(4), 487-503. <https://doi.org/10.12989/scs.2021.41.4.487>.
- Bounouara, F., Aldosari, S.M., Chikh, A., Kaci, A., Bousahla, A.A., Bourada, F., ... & Albalawi, H. (2023), "The effect of visco-Pasternak foundation on the free vibration behavior of exponentially graded sandwich plates with various boundary conditions", *Steel Compos. Struct.*, **46**(3), 367-383. <https://doi.org/10.12989/scs.2023.46.3.367>.
- Chakraverty, S., Jindal, R. and Agarwal, V.K. (2005), "Flexural vibrations of non-homogeneous elliptic plates", *Int. J. Eng. Mat. Sci.*, **12**, 521-528.
- Chen, W.Q., Lee, K.Y. and Ding, H.J. (2005), "On free vibration of non-homogeneous transversely isotropic magneto-electro-elastic plate", *J. Sound Vib.*, **279**, 237-251. <https://doi.org/10.1016/j.jsv.2003.10.033>.
- Dastjerdi, S., Malikan, M. and Dimitri, R. (2021), "Nonlocal elasticity analysis of moderately thick porous functionally graded plates in a hygro-thermal environment", *Compos. Struct.*, **225**, 112925. <https://doi.org/10.1016/j.compstruct.2020.112925>.
- Djilali, N., Bousahla, A.A., Kaci, A., Selim, M.M., Bourada, F., Tounsi, A., ... & Mahmoud, S.R. (2022), "Large cylindrical deflection analysis of FG carbon nanotube-reinforced plates in thermal environment using a simple integral HSDT", *Steel Compos. Struct.*, **42**(6), 779-789. <https://doi.org/10.12989/scs.2022.42.6.779>.

- Eringen, A.C. (1981), "Theory of nonlocal thermoelasticity", *Int. J. Eng. Sci.*, **12**(12), 1063-1077. [https://doi.org/10.1016/0020-7225\(74\)90033-0](https://doi.org/10.1016/0020-7225(74)90033-0).
- Fesharaki, J.J., Fesharaki, V.J., Yazdipoor, M. and Razavian, B. (2012), "Two dimensional solution of electro mechanical behavior of functionally graded piezoelectric hollow cylinder", *Appl. Math. Model.*, **36**, 5521-5533. <https://doi.org/10.1016/j.apm.2012.01.01>.
- Gawin, D., Majorana, C.E. and Scherfler, B.A. (1999), "Numerical analysis of hygro thermal behavior and damage of concrete at high temperature", *Mech. Cohes.-frict. Mater.: J. Exper. Model. Comput. Mater. Struct.*, **4**, 37-74. [https://doi.org/10.1002/\(SICI\)1099-1484\(199901\)4:1<37::AID-CFM58>3.0.CO;2-S](https://doi.org/10.1002/(SICI)1099-1484(199901)4:1<37::AID-CFM58>3.0.CO;2-S).
- Hadji, M., Bouhadra, A., Mamen, B., Menasria, A., Bousahla, A.A., Bourada, F., ... & Tounsi, A. (2023), "Combined influence of porosity and elastic foundation parameters on the bending behavior of advanced sandwich structures", *Steel Compos. Struct.*, **46**(1), 1-13. <https://doi.org/10.12989/scs.2023.46.1.001>.
- Hebali, H., Chikh, A., Bousahla, A.A., Bourada, F., Tounsi, A., Benrahou, K.H., ... & Tounsi, A. (2022), "Effect of the variable visco-Pasternak foundations on the bending and dynamic behaviors of FG plates using integral HSDT model", *Geomech. Eng.*, **28**(1), 49-64. <https://doi.org/10.12989/gae.2021.28.1.049>.
- Hou, P.F., Andrew, Y.T. and Leung, H. (2008), "Point heat source on the surface of a semi-infinite transversely isotropic electro-magneto-thermo-elastic material", *Int. J. Eng. Sci.*, **46**, 273-285. <https://doi.org/10.1016/j.ijengsci.2007.11.006>.
- Hutchinson, J.R. (1979), "Axisymmetric flexural vibrations of a thick free circular plate", *J. Appl. Mech.*, **46**, 139-144. <https://doi.org/10.1115/1.3424485>.
- Janson, K.M.B., Zhang, M.F. and Ernst, L.J. (2020), "Effect of temperature and humidity on moisture diffusion in an epoxy moulding compound material", *Micro. Reliab.*, **107**, 113596. <https://doi.org/10.1016/j.microrel.2020.113596>.
- Jiyangi, C., Hualing, C. and Ernian, P. (2006), "Free vibration of functionally graded, magneto-thermo-electro-elastic and multilayered plates", *Acta Mechanica Solida Sinica*, **19**, 60-66. <http://doi.org/10.1007/s10338-006-0619-3>.
- Kakar, R. (2013), "Magneto elastic torsional surface waves in prestressed fiber reinforced medium", *Int. J. Math. Mech.*, **9**, 1-19.
- Kallavanar, V., Kattimani, S. and Elahi, M. (2021), "Neural network-based prediction model to investigate the influence of temperature and moisture on vibration characteristics of skew laminated composite sandwich plates", *Mater.*, **14**(12), 3170. <https://doi.org/10.3390/ma14123170>.
- Kouider, D., Kaci, A., Selim, M.M., Bousahla, A.A., Bourada, F., Tounsi, A., ... & Hussain, M. (2021), "An original four-variable quasi-3D shear deformation theory for the static and free vibration analysis of new type of sandwich plates with both FG face sheets and FGM hard core", *Steel Compos. Struct.*, **41**(2), 167-191. <http://doi.org/10.12989/scs.2021.41.2.167>.
- Lata, P. and Singh, S. (2022), "Effect of rotation and inclined load in a nonlocal magnetothermoelastic solid with two temperature", *Adv. Mater. Res.*, **11**(1), 23-39. <https://doi.org/10.12989/amr.2022.11.1.023>.
- Loghman, A., Nasar, M. and Arefi, M. (2017), "Non symmetric thermo mechanical analysis of a functionally graded cylinder subjected to mechanical, thermal and magnetic loads", *J. Therm. Stress.*, **40**, 765-782. <https://doi.org/10.1080/01495739.2017.1280380>.
- Mehditabar, A., Rahimi, G.H. and Tarahhomi, M.H. (2018), "Thermo-elastic analysis of a functionally graded piezoelectric rotating hollow cylindrical shell subjected to dynamic loads", *Mech. Adv. Mater. Struct.*, **25**(12), 1068-1079. <https://doi.org/10.1080/15376494.2017.1329466>.
- Mesbah, A., Belabed, Z., Amara, K., Tounsi, A., Bousahla, A.A. and Bourada, F. (2023), "Formulation and evaluation a finite element model for free vibration and buckling behaviours of functionally graded porous (FGP) beams", *Struct. Eng. Mech.*, **86**(3), 291-309. <https://doi.org/10.12989/sem.2023.86.3.291>.
- Mudhaffar, I.M., Chikh, A., Tounsi, A., Al-Osta, M.A., Al-Zahrani, M.M. and Al-Dulaijan, S.U. (2023), "Impact of viscoelastic foundation on bending behavior of FG plate subjected to hygro-thermo-mechanical loads", *Struct. Eng. Mech.*, **86**(2), 167-180. <https://doi.org/10.12989/sem.2023.86.2.167>.
- Mudhaffar, I.M., Tounsi, A., Chikh, A., Al-Osta, M.A., Al-Zahrani, M.M. and Al-Dulaijan, S.U. (2021), "Hygro-thermo-mechanical bending behavior of advanced functionally graded ceramic metal plate resting on a viscoelastic foundation", *Struct.*, **33**, 2177-2189. <https://doi.org/10.1016/j.istruc.2021.05.090>.

- Nagaya, K. (1974), "Simplified method for solving problems of vibrating plates of doubly connected arbitrary shape", *J. Sound Vib.*, **74**, 553-564. [https://doi.org/10.1016/0022-460X\(81\)90418-1](https://doi.org/10.1016/0022-460X(81)90418-1).
- Nagaya, K. (1980), "Method for solving vibration problems of a plate with arbitrary shape", *J. Acoust. Soc. Am.*, **67**, 2029-2033. <https://doi.org/10.1121/1.384444>.
- Nagaya, K. (1981), "Dispersion of elastic waves in bars with polygonal cross section", *J. Acoust. Soc. Am.*, **70**, 763-770. <https://doi.org/10.1121/1.386914>.
- Pan, E. (2001), "Exact solution for simply supported and multilayered magneto-electro-elastic plates", *J. Appl. Mech.*, **68**, 608-618. <https://doi.org/10.1115/1.1380385>.
- Ramu, I., Narendra, M. and Venu, M. (2018). "Effect of hygrothermal environment on free vibration characteristics of FGM plates by finite element approach", *IOP Conf. Ser.: Mater. Sci. Eng.*, **377**(1), 012021. <http://doi.org/10.1088/1757-899X/377/1/012021>.
- Reddy, J.N. and Chin, C.D. (2007), "Thermo mechanical analysis of functionally graded cylinders and plates", *J. Therm. Stress.*, **21**, 593-626. <https://doi.org/10.1080/01495739808956165>.
- Selvamani, R. (2015), "Wave propagation in a rotating disc of polygonal cross-section immersed in an inviscid fluid", *Cogent Eng.*, **2**(1), 1002162. <https://doi.org/10.1080/23311916.2014.1002162>.
- Selvamani, R. (2016), "Influence of thermo-piezoelectric field in a circular bar subjected to thermal loading due to laser pulse", *Mater. Phys. Mech.*, **27**, 1-8.
- Selvamani, R. (2017), "Stress waves in a generalized thermo elastic polygonal plate of inner and outer cross sections", *J. Solid Mech.*, **9**(2), 263-275.
- Selvamani, R. and Infant Sujitha, G. (2018a), "Effect of non homogeneity in a magneto electro elastic plate of polygonal cross sections", *Mater. Phys. Mech.*, **40**(1), 1-24. http://doi.org/10.18720/MPM.4012018_11.
- Selvamani, R. and Ponnusamy, P. (2013), "Elasto dynamic wave propagation in a transversely isotropic piezoelectric circular plate immersed in fluid", *Mater. Phys. Mech.*, **17**(2), 164-177.
- Selvamani, R. and Ponnusamy, P. (2013), "Generalized thermoelastic waves in a rotating ring shaped circular plate immersed in an inviscid fluid", *Mater. Phys. Mech.*, **18**(1), 77-92. <https://doi.org/10.1115/1.1380385>.
- Selvamani, R. and Ponnusamy, P. (2015), "Wave propagation in a generalized piezothermoelastic rotating bar of circular cross section", *Multidisc. Model. Mater. Struct.*, **11**(2), 216-237. <https://doi.org/10.1108/MMMS-06-2014-0038>.
- Selvamani, R. and Sujitha, G.I. (2018), "Wave propagation in a non-homogeneous magneto-thermo-electro-elastic disc of polygonal cross sections immersed in an inviscid fluid", *J. Phys.: Conf. Ser.*, **1139**(1), 012013. <http://doi.org/10.1088/1742-6596/1139/1/012013>.
- Singh, B. and Bijarnia, R. (2020), "Nonlocal effects on propagation of waves in a generalized thermoelastic solid half space", *Struct. Eng. Mech.*, **7**(4), 473-479. <https://doi.org/10.12989/sem.2021.77.4.473>.
- Singh, S. and Lata, P. (2020), "Effects of nonlocality and two temperature in a nonlocal thermo elastic solid due to ramp type heat source", *Arab J. Basic Appl. Sci.*, **27**(1), 358-364. <https://doi.org/10.1080/25765299.2020.1825157>.
- Tounsi, A., Mostefa, A.H., Attia, A., Bousahla, A.A., Bourada, F., Tounsi, A. and Al-Osta, M.A. (2023), "Free vibration investigation of functionally graded plates with temperature-dependent properties resting on a viscoelastic foundation", *Struct. Eng. Mech.*, **86**(1), 1-16. <https://doi.org/10.12989/sem.2023.86.1.001>.
- Vinyas, M. and Kattimani, S.C. (2017), "Hygrothermal analysis of magneto-electro-elastic plate using 3D finite element analysis", *Compos. Struct.*, **180**, 617-637. <https://doi.org/10.1016/j.compstruct.2017.08.015>.
- Vinyas, M. and Kattimani, S.C. (2018), "Finite element evaluation of free vibration characteristics of magneto-electro-elastic rectangular plates in hygrothermal environment using higher order shear deformation theory", *Compos. Struct.*, **202**, 1339-1352. <https://doi.org/10.1016/j.compstruct.2018.06.069>.
- Vinyas, M., Kattimani, S.C. and Joladarashi, S. (2018), "Hygrothermal coupling analysis of magneto-electroelastic beams using finite element methods", *J. Therm. Stress.*, **40**, 1063-1079. <https://doi.org/10.1080/01495739.2018.1447856>.
- Wang, W., Dong, X.K. and Wang, X.Y. (2004), "Hygro thermal effect on dynamic inter laminar stresses in

- laminated plates with piezoelectric actuators”, *Compos. Struct.*, **71**(2), 220-228. <https://doi.org/10.1016/j.compstruct.2004.10.004>.
- Zaitoun, M.W., Chikh, A., Tounsi, A., Al-Osta, M.A., Sharif, A., Al-Dulaijan, S.U. and Al-Zahrani, M.M. (2022), “Influence of the visco-Pasternak foundation parameters on the buckling behavior of a sandwich functional graded ceramic–metal plate in a hygrothermal environment”, *Thin Wall. Struct.*, **170**, 108549. <https://doi.org/10.1016/j.tws.2021.108549>.
- Zenkour, A.M. (2012), “Piezoelectric behavior of an inhomogeneous hollow cylinder with thermal gradient”, *Int. J. Thermophys.*, **33**, 1288-1301. <https://doi.org/10.1007/s10765-012-1248-3>.
- Zhang, X.M. and Yu, J.G. (2013), “Effects of initial stresses on guided waves in unidirectional plates”, *Arch. Mech.*, **65**(1), 3-26.

Appendix

$$U_n^1 = 2\{\beta(\beta - 1)J_\beta(Nr) \cos n\theta + (Nr)J_{\beta+1}(Nr) \cos n\theta\} \cos 2(\theta - \gamma_i) \\ - r^2\{N^2(\lambda + 2 \cos^2(\theta - \gamma_i))J_\beta(Nr)\} \cos n\theta$$

$$U_n^2 = \{n(\delta - 1)J_\delta(\wp r) - (\wp r)J_\delta(\wp r)\} \cos 2(\theta - \gamma_i) \cos n\theta - \{(\delta(\delta + 2) + n^2 - \\ (\wp r)^2) \frac{J_\delta(\wp r)}{2} - (\wp r)J_{\delta+1}(\wp r)\} \sin n\theta \sin 2(\theta - \gamma_i)$$

$$V_n^1 = [2\{\beta J_\beta(Nr) \cos n\theta - (Nr)J_{\beta+1}(Nr) \cos n\theta\} + ((Nr)^2 - \beta^2 - \\ n^2) \cos n\theta J_\beta(Nr)] \sin 2(\theta - \gamma_i) + 2n\{(\beta - 1)J_\beta(Nr) \sin n\theta - \\ (Nr)J_{\beta+1}(Nr) \sin n\theta\} \cos 2(\theta - \gamma_i)$$

$$V_n^2 = 2n[\delta J_\delta(\wp r) \cos n\theta - (\wp r)J_{\delta+1}(\wp r) \cos n\theta] \sin 2(\theta - \gamma_i) + 2\{[\delta J_\delta(\wp r) \sin n\theta - \\ (\wp r)J_{\delta+1}(\wp r) \sin n\theta] + [(\wp r)^2 - \delta^2 - n^2] \sin n\theta J_\delta(\wp r)\} \cos 2(\theta - \gamma_i)$$

$$Y_n^1 = \{nJ_n(ar) - (ar)J_{n+1}(ar)\} \cos n\theta$$

$$Y_n^2 = nJ_n(ar) \cos n\theta$$

$$\overline{U}_n^1 = 2\{\beta(\beta - 1)J_\beta(Nr) \sin n\theta + (Nr)J_{\beta+1}(Nr) \sin n\theta\} \sin 2(\theta - \gamma_i) - r^2\{N^2(\lambda + \\ 2 \cos^2(\theta - \gamma_i))J_\beta(N) \sin n\theta$$

$$\overline{U}_n^2 = \{n(\delta - 1)J_\delta(\wp r) \sin n\theta - (\wp r)J_\delta(\wp r) \sin n\theta\} \sin 2(\theta - \gamma_i) - \{(\delta(\delta + 2)) + n^2 - \\ (\wp r)^2) \frac{J_\delta(\wp r)}{2} \cos n\theta - (\wp r)J_{\delta+1}(\wp r)\} \cos 2(\theta - \gamma_i)$$

$$\overline{V}_n^1 = [2\{\beta J_\beta(Nr) \sin n\theta - (Nr)J_{\beta+1}(Nr) \sin n\theta\} + ((Nr)^2 - \beta^2 - n^2) \sin n\theta J_\beta(Nr)] \cos 2(\theta - \\ \gamma_i) + 2n\{(\beta - 1)J_\beta(Nr) \cos n\theta - (Nr)J_{\beta+1}(Nr) \cos n\theta\} \sin 2(\theta - \gamma_i).$$

$$\overline{V}_n^2 = 2n[\delta J_\delta(\wp r) \sin n\theta - (\wp r)J_{\delta+1}(\wp r) \sin n\theta] \cos 2(\theta - \gamma_i) + 2\{[\delta J_\delta(\wp r) - \\ (\wp r)J_{\delta+1}(\wp r)] + [(\wp r)^2 - \delta^2 - n^2]J_\delta(\wp r)\} \cos n\theta \sin 2(\theta - \gamma_i)$$

$$\overline{Y}_n^1 = \{nJ_n(ar) - (ar)J_{n+1}(ar)\} \sin n\theta$$

$$\overline{Y}_n^2 = nJ_n(ar) \sin n\theta$$

$$U_n^3 = 0, U_n^4 = 0, V_n^3 = 0, V_n^4 = 0$$